Turbulent Velocity Spectra from Laser Doppler Data

C. Tropea*, H. Nobach*, A. Ramond†, Ph. Reulet†

*Technical University Darmstadt
†ONERA

Abstract This contribution reviews the estimation of spectra from laser Doppler data and provides some recommended guidelines. It is shown that reliable spectral estimates can be achieved for frequencies well beyond the mean data rate. The estimators discussed here exhibit some further advantages when used for processing data from multi-point measurements, used for spatial correlations. Some final remarks are directed towards the ramifications of these procedures on the optical system design.

1 Introduction

Laser measurement techniques are particularly attractive in aerodynamic research because they are both non-intrusive and quantitative. The range of available techniques has expanded rapidly in recent years, as indicated in Fig. 1. This figure uses a classification according to components (u, v, w, d_{p}) and dimensions (x, y, z, t) and has been restricted to those techniques employing elastic light scattering from tracer particles.

While multi-component techniques such as PIV or DGV provide valuable spatial information about the flowfield, these techniques are generally quite limited in their temporal resolution. This limitation is closely coupled to the readout speed of the CCD cameras used for detection. From Fig. 1 it is evident that at the present time only the laser Doppler/phase Doppler techniques offer this time resolution.

High time resolution can be important in two respects. The first is to be able to resolve instationary or periodic phenomena and the second is to provide spectral (or correlation) information about the flow process. It is the latter feature, which is the focus of the present paper.

Spectral estimation of flow velocity fluctuations from laser Doppler data has been a topic of discussion since the early work of Mayo *et al* [15]. An historical summary and also a review of the present state-of-the-art has been published recently by Benedict *et al* [4]. The estimation is not straightforward due to several unique features of laser Doppler data, which are briefly reviewed in section 2. In sections 3.1.1 and 3.1.2 the two most recommendable estimators are presented, including some very recent improvements. The situation becomes one degree more complex when multi-component or multi-point measurements are involved and this is discussed in section 3.2.

Spectral estimation is often a first step to estimation of further quantities such as length scales or dissipation. Section 4 shows how some of these quantities can

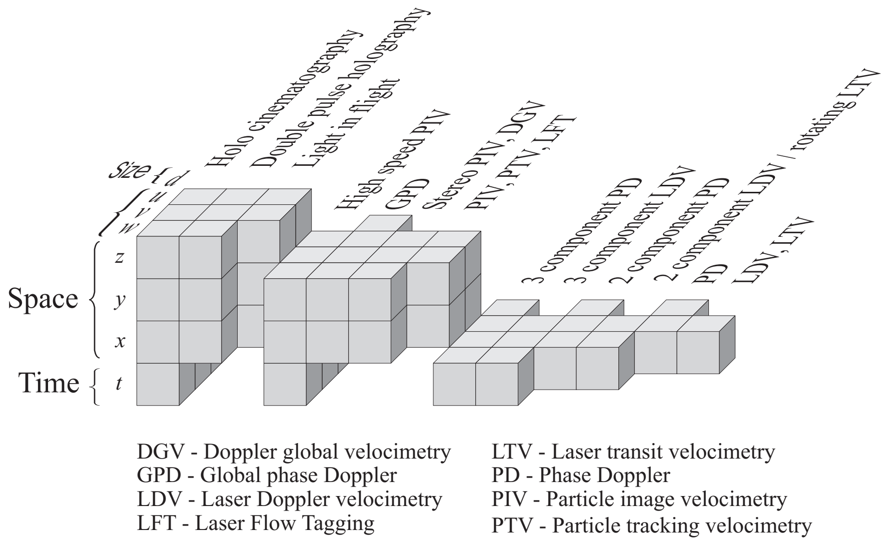

Figure 1: Overview of laser measurement techniques for single and multi-phase flows

be computed.

2 Characteristics of Laser Doppler Data

For the present discussion no details of the laser Doppler technique itself will be given. It is simply assumed that the device makes available a data set consisting of up to three velocity components and an arrival time for every tracer particle in the flow which has been detected and validated. Thus, primarily only processing algorithms (software) are considered.

The laser Doppler technique gives a transient history of velocity values derived from individual particles that cross the measurement volume. For each velocity measurement there exists an arrival time of the corresponding particle. The laser Doppler data set represents a series of time-velocity pairs.

2.1 Stochastic sampling

The most important feature of the laser Doppler data set arises from the fact that the technique is a tracer-based method, hence the data sample arival times are irregular. In [6, 7] investigations on the sampling statistics have been presented. Presuming an equal particle distribution in space with a constant concentration c_s, the intervals Δt between the measurements are distributed exponentially

$$p(\Delta t) = \dot{n} e^{-\dot{n}\Delta t} \tag{1}$$

with the mean data rate $\dot{n}$ (Figure 2).

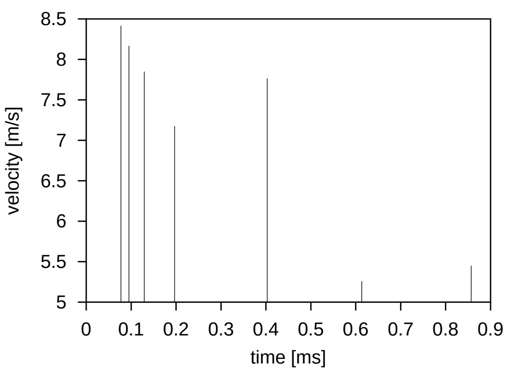

Figure 2: Stochastic sampling with a laser Doppler instrument

The exponential distribution means that regardless of how low the mean data rate is, the most probable time between samples remains zero. Principally, information about high frequency velocity fluctuations is therefore always available.

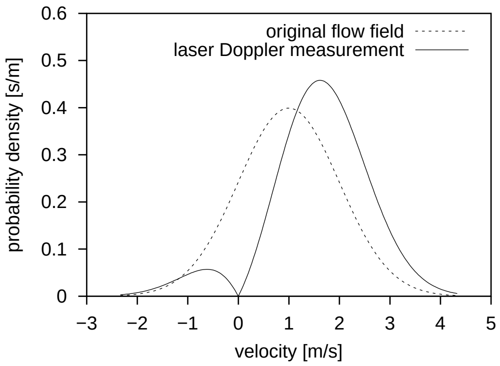

Figure 3: Velocity distribution of the original flow field compared to the data set (1 dimensional simulation)

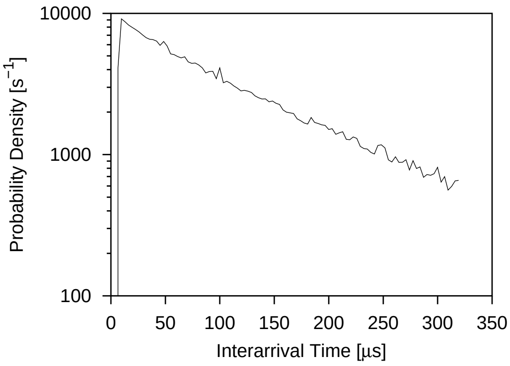

Figure 4: Distribution of interarrival times (measurement)

2.2 Correlation between velocity and data rate

For non-constant velocities the instantaneous data rate is not constant in spite of a constant particle concentration c_s. Presuming a constant spatial distribution of tracer particles the fluid or gas volume that passes the measurement volume within a given time is proportional to the velocity, hence the rate of measurements is proportional to the velocity as well. This leads to a more frequent occurrence of high velocity measurements and to a distorted velocity distribution, called velocity bias. This effect is shown schematically in Figure 3.

Furthermore, the data rate depends on the size of the measurement volume. It is proportional to the projected area $A_\perp$ of the measurement volume normal to the flow velocity vector. Because of the significant prolate shape of the measurement volume, the size of the projection depends on the direction of the flow. An expression of the variable data rate is given through

$$\dot{n} = c_s A_\perp(\vec{u}) \, |\vec{u}| \tag{2}$$

which describes the correlation of the data rate and the velocity [21]. Consequently, the sampling scheme depends on the measured velocity value.

2.3 Processor delay

The velocity measurements ensue normally from single particles. If two particles enter the measurement volume within a short time interval, the burst signals overlap. Because of the phase difference of the bursts a phase drift can be seen within the double burst signal. Therefore, the burst frequency cannot be derived exactly. These multi-particle signals are detected by pre-processors that often reject them from the data stream. This leads to a significant underrepresentation of small interarrival times (Figure 4). Note that even modern and fast processors cannot avoid the delay time, since it is given by the optical setup through the simple approximation

$$t_{\mathrm{del}} = \frac{d_{\mathrm{MV}}}{\bar{u}} \tag{3}$$

using the diameter of the measurement volume d_{MV} and the mean velocity $\bar{u}$.

2.4 Noise

There are numerous sources of noise both in the velocity values registered as well as in the arrival times. These include the stochastic nature of light generation, scattering and detection [15], electronic noise [5] and also noise due to the random arrival of particles in the detection volume [11]. Noise in the processed signal leads to fluctuations in the measured velocity values, which cannot be distiguished from turbulent flow fluctuations. However, it is generally assumed that velocity fluctuations due to noise are random in nature, i. e. lead to white noise in the spectral domain of velocity fluctuations.

3 Estimation of correlation and power spectral density functions

3.1 One-point, one-component measurements

The fact that, due to the exponetially distributed interarrival times, velocity information is often available over very short time spans, suggests that principally, information about very high frequency fluctuations is contained in the data. This is in strong contrast to data which is sampled at equal time intervals, for which the sampling theorem applies and for which no information above the Nyquist frequency ($f_c = \frac{1}{2\Delta t}$, Δt sample interval) is available. This, incidently, was the motivation for a series of articles investigating the possibility of a direct Fourier transform of the laser Doppler data to obtain a PSD (power spetral density) estimate, i. e. a transform without exploiting the FFT [9, 10, 28].

However, the prospect of alias-free PSD estimators at frequencies beyond the mean Nyquist frequency ($f_c = \dot{n}/2$) through use of a direct transform did not meet expectations. Basically the variability of the estimator increased too quickly with frequency, so that while an estimation could formally be performed at high frequencies, the answer was extremely unreliable. In [31] Tummers and

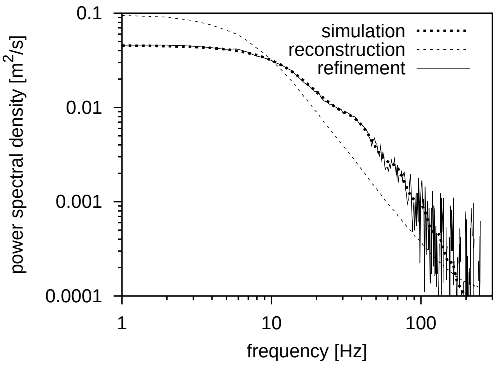

Figure 5: The "particle-rate filter" and the refinement using the SH reconstruction (simulation)

Passchier have shown that its variability, even with block averaging, is no better than the slotting algorithm discussed below. Furthermore, even with further modifications [30, 27, 29, 20], the estimation variance is larger then the variance of the slotting technique or the refined reconstruction. This estimator is therefore not pursued there and is only presented occasionally in the literature as a comparison.

3.1.1 Reconstruction

Reconstruction approaches create equidistant spaced time series by resampling according to various interpolation schemes, thereby allowing an FFT to be used in making PSD estimates. The most common scheme by far is the sample-and-hold (zero-order, SH) reconstruction. This is the simplest of the polynomial class of reconstruction algorithms. The limits of the reconstruction technique are given through the data rate, since the reconstruction from irregularly sampled data sets has a filter characteristic [1] (figure 5). It has been well documented that the filter effect becomes significant at frequencies even under $\dot{n}/2\pi$ [18]. Recently, a refinement was developed that cancels the filter effect associated with reconstruction techniques [25] (figure 5). The approach is to derive an expression for the resampled ACF in terms of the true ACF. The relation is then inverted to improve the ACF estimation. In the case of the SH reconstruction the refinement becomes very simple

$$\hat{R}_k = \begin{cases} \hat{R}'_0 & \text{for } k=0 \\ (2c+1)\hat{R}'_k - c\left(\hat{R}'_{k-1}+\hat{R}'_{k+1}\right) & \text{for } k=1\ldots K \end{cases} \tag{4}$$

$$c = \frac{\mathrm{e}^{-\dot{n}\Delta\tau}}{\left(1-\mathrm{e}^{-\dot{n}\Delta\tau}\right)^2} \tag{5}$$

where $\hat{R}$ is the refined ACF estimate based on the ACF $\hat{R}'$ of the reconstructed and resampled time signal. In principle, a refinement can be derived for any reconstruction algorithm. Other reconstruction techniques, such as single exponential reconstruction [14], other proportional one-point reconstructions [25] or even the linear reconstruction, and their refinement filters have been investigated. The results are similar and the algorithm is effective enough with the SH reconstruction that the advantages of other reconstruction schemes become negligible. Therefore, the SH reconstruction is sufficient and furthermore, the refinement filter becomes very simple only for this reconstruction scheme.

The influence of the velocity bias on the results of the reconstruction technique is small (at least for quite high data rates), because the reconstruction values with large interarrival times are resampled more often than values with smaller interarrival times. This principle is similar to the arrival time weighting [2].

However, the noise and the processor delay affect the statistics of this estimator. Especially the value $\hat{R}_0$ of the ACF at lag time zero is obscured by these effects. To remove the noise and the effect of the processor delay from the ACF estimate, a model-based estimation of $\hat{R}_0$ can be used. Principally speaking, simple and convenient models [17, 22] can be used. Nevertheless, the parameter optimization is difficult and costly. The use of a weighting function with strong coefficients close to the lag time zero allows simpler models to be used. In [19] a Gaussian function and in [4] a more flexible version with an additional parameter was used as a model of the ACF. These models correspond to the Taylor microscale estimation (parabolic behavior of R near $\tau = 0$). However, these models are not able to describe periodic components, so that the weighting function should decrease very strong with the lag time. Figure 6 shows the effect of the model-based variance estimation.

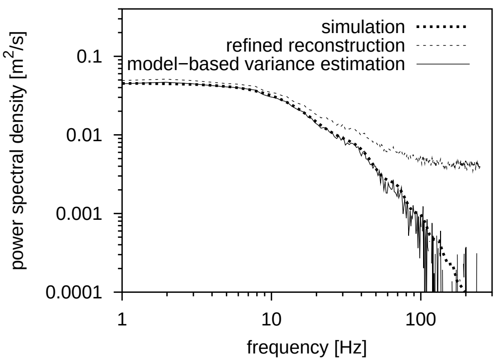

Figure 6: The effect of the data noise and the processor delay on the PSD and the result with the model-based variance estimation using the reconstruction algorithm (simulation)

The corrected ACF estimate can be transformed to the PSD using the discrete cosine transform

$$\hat{S}_j = \hat{S}(f_j) = \hat{S}\left(\frac{j}{2K\Delta\tau}\right) = 2\Delta\tau \times \left[\hat{R}_0 + 2\sum_{k=1}^{K-1}\hat{R}_k\cos(2\pi f_j k\Delta\tau) + (-1)^j\hat{R}_K\right] \tag{6}$$

Alternatively, in [31] a frequency dependent variable windowing of the ACF is recommended for the transform to the PSD

$$\hat{S}(f) = 2\Delta\tau \left[\hat{R}_0 + 2\sum_{k=1}^{K-1} d_k(f)\hat{R}_k \cos(2\pi f k\Delta\tau)\right] \quad (7)$$

with windowing coefficients $d_k(f)$, which vary with the frequency f. Good experience was obtained using the Tukey-Hanning window with

$$d_k(f) = \begin{cases} \frac{1}{2} + \frac{1}{2}\cos\left(\frac{\pi f k\Delta\tau}{\kappa}\right) & \text{for } |fk\Delta\tau| < \kappa \\ 0 & \text{otherwise} \end{cases} \quad (8)$$

The parameter κ can be chosen arbitrarily, e. g. $\kappa = 6$ was found to yield good results.

This technique reduces the estimation variance especially for higher frequencies, while through the windowing a leakage effect arises. However, now the spectrum can be calculated at any frequency. This could reduce the number of required spectral lines in the case of a logarithmic axis scaling, which is often used to present turbulence spectra. This is important because the the FFT cannot be used for this transform and every spectral value has to be calculated independently.

Recently, the capability of the refined reconstruction algorithm was demonstrated using experimental data taken behind a grind in a wind tunnel [12]. The algorithm could be verified to be bias free and to be able to recover the PSD up to frequencies much higher than the mean data rate.

3.1.2 Slotcorrelation

To reduce the variability of the original slotting algorithm [15], the local normalization [19] and the fuzzy slotting technique [26] were combined to a more powerful algorithm [16]. Additionally, the algorithm was extended by weighting algorithms [24] known from the estimation of statistical values like the mean velocity or the variance [8]. The advantage of this algorithm is the very low variability of the estimate and the possibility of reducing the influence of the velocity bias by several, different weighting techniques.

Every combination of two samples u_i and u_j of the data series taken at the times t_i and t_j is processed for each time lag $k\Delta\tau$ ($k = 0 \ldots K$) using

$$\hat{R}_k = \frac{\hat{\sigma}_\mathrm{u}^2 A}{\sqrt{BC}} \quad (9)$$

with

$$A = \sum_{i=1}^{N-1}\sum_{j=i+1}^{N} u_i u_j w_i w_j b_k(t_j - t_i) \quad (10)$$

$$B = \sum_{i=1}^{N-1}\sum_{j=i+1}^{N} u_i^2 w_i w_j b_k(t_j - t_i) \quad (11)$$

$$C = \sum_{i=1}^{N-1}\sum_{j=i+1}^{N} u_j^2 w_i w_j b_k(t_j - t_i) \quad (12)$$

and with the fuzzy mask function

$$b_k(t_j - t_i) = \begin{cases} 1 - \left|\frac{t_j - t_i}{\Delta\tau} - k\right| & \text{for } \left|\frac{t_j - t_i}{\Delta\tau} - k\right| < 1 \\ 0 & \text{otherwise} \end{cases} \quad (13)$$

The estimate of the velocity variance is obtained using

$$\hat{\sigma}_\mathrm{u}^2 = \frac{\sum_{i=1}^{N} u_i^2 w_i}{\sum_{i=1}^{N} w_i}. \quad (14)$$

with the weighting factors w_i.

To obtain the weighting factors several schemes can be used. Example weighting factors, w_i, are the transit time weighting [13]

$$w_i = \mathrm{TT}_i \quad (15)$$

or the arrival time weighting [2]

$$w_i = t_i - t_{i-1} \quad (16)$$

with the arrival time t_i of the velocity sample u_i, which is independent of the particle distribution [8]. Both of these weighting functions are found to yield non-biased results for accurate measurements of the transit time (transit time weighting) or sufficiently high data densities (interarrival time weighting).

Note that the estimation of the correlation function (Eq. (9)) in the case of interarrival time weighting requires a revised scheme, the forward-backward weighting [24]

$$
\begin{aligned}
w_i &= t_i - t_{i-1} && (17)\\
w_j &= t_{j+1} - t_j && (18)
\end{aligned}
$$

because of the correlation between the time lag and the arrival time distribution.

In principal, also a velocity weighting [21] can be used. however, it was found to be very sensitive to the noise in the data set.

Since self-products are not taken, the A value in the numerator of equation (9) is independent of the data noise. However, the coefficients in the denuminator include self-products and are affected by the data noise. Furthermore, also the processor delay influences the estimation results. Therefore, the model-based variance estimation used for the refined reconstruction can be used here to improve the results of the slotting algorithm. The transform to the PSD is similar to the procedure given for the refined reconstruction. It can be performed either without or with the variable windowing technique to improve the spectrum.

3.2 Multi-component/multi-point measurements

The slotting technique and the refined reconstruction have been modified to estimate also the cross-correlation function (CCF) and the cross-power spectral density (CPSD) from multi-channel laser Doppler measurements [23, 26]. Both arrangements of measurment volumes are possible, the multi-component and the multi-point configuration.

In the multi-component configuration the measurement volumes overlap, yielding different velocity components of the flow at a common location. The cross-correlation of the different velocity components represent components of the Reynolds shear stress tensor.

Normally, the data of the two or more individual laser Doppler systems are accepted only if the measurements of all velocity components occur within a small time window (coincidence). Then the individual velocity measurements can be assigned to *one* particle and the velocity vector of each particle can be transformed to any other coordinate system.

In [23] a coordinate transform is derived also for free-running multi-component measurements without coincidence. In that case, first the CCF must be calculated in the coordinates of the measurement system. The transform to another coordinate system can then be done only for the CCF, not for the individual particles.

The CCF can be calculated from the data sets either with the slotting or the reconstruction technique. Both techniques can be easily adapted to measurements in either the free-running or the coincidence mode. The advantage of the free-running mode is the higher data rate, since all particles are accepted passing at least one of the measurement volumes, while with the requirement of coincidence, only particles are validated which pass through *all* measurement volumes. On the other hand, the coincidence reduces the effective size of the measurement volume, leading to a higher spatial resolution of the system, while without the coincidence the velocities are averaged over the union of all individual measurement volumes.

If a two-point or multi-point laser Doppler system is considered, the correlations represent spatial correlations. Most commonly, these correlations between velocity fluctuations are evaluated at lag time zero (covariance or after normalization correlation coefficient), however in principle all lag times can be considered, in which case the correlation function or space-time correlation function between velocity fluctuations can be obtained.

There are three basic deficiencies in present laser Doppler systems which can be eliminated using the new estimators for cross-correlations. The first concerns the need for coincidence. Conventional estimators of the cross-correlation function work directly from the definition

$$R_{AB}(\tau) = \frac{1}{N}\sum_{i=1}^{N} u_A(t_i)u_B(t_i+\tau) \quad (19)$$

whereby it is understood that the mean has been removed from the input signals u_A and u_B. Thus a product $u_A u_B$ can only contribute to the sum if velocity information from the two channels come with a lag time of exactly τ. Practically, an acceptance window in time (coincidence window) is tolerated, however in many applications this window must be chosen very narrow to avoid a loss of correlation, hence a biased estimator. Physically, the required window width will be dictated by the time correlation function itself, and must often be chosen empirically and/or iteratively.

In any case, given a narrow coincidence window, the data rate of coincident velocity pairs may become very low, especially for spatially separated measurement volumes. Thus, the duration of the measurement to achieve a statistically satisfactory number of samples N may become intolerably long. Accepting a lower value of N simply increases the variance of the estimate.

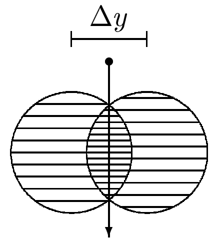

Figure 7: Two-point configuration leading to spatial bias of the cross-correlation funtion.

A second deficiency concerns the coincidence window implementation, which is available at the hardware level only for $\tau = 0$. In this case only data pairs which occur simultaneous in time are actively acquired, minimizing the amount of collected data. For other time lags ($\tau \neq 0$) no hardware coincidence is forseen. If the function $R_{AB}(\tau)$ is to be evaluated at many τ values, then all data must be acquired from both channels and coincidence must be implemented at the software level. In this case, again, due to the generally lower 'hit' rate of coincidence, large amounts of data must be acquired and recorded to yield statistically secure estimates.

A final difficulty with present estimators has been pointed out by Benedict and Gould [3] in their discussion of two-point correlation estimates when the separation distance becomes very small. Such measurements are necessary if direct measurements of dissipation are to be attempted. Once the two measurement volumes begin to overlap any g-type correlation will become biased because coincidence will be triggered when a single particle passes through the overlapping region, as illustrated in figure 7. However velocity data from the two channels does not originate from the surmised spatial separation of Δy, but with an effective spatial separation of *zero*.

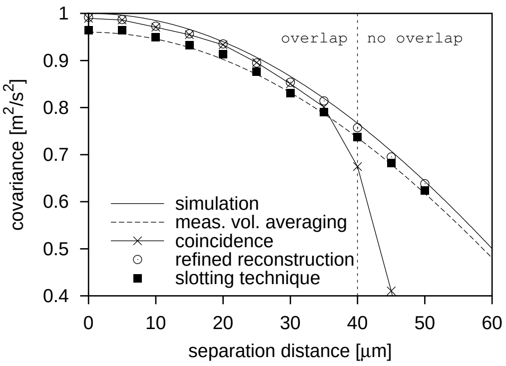

Figure 8: Covariance estimation for the two-point f-type configuration.

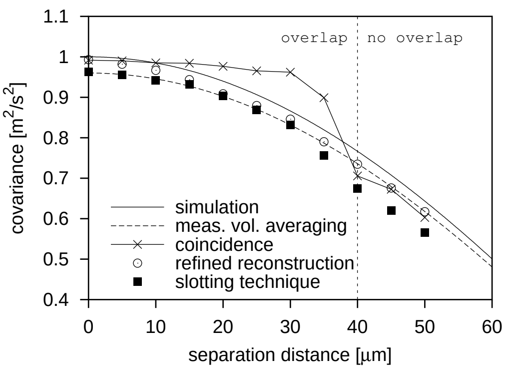

Figure 9: Covariance estimation for the two-point g-type configuration.

Thus the estimator using coincidence will lead to a spatial bias in the near-field region. This bias is very significant, since the number of single particle, two-channel signals is much larger than for two-particle, two-channel coincident signals. All of the above difficulties will be alleviated using the reconstruction or the slotting method for multi-channel measurements in the free-running mode. Furthermore, if necessary, coordinate transforms can be performed with the derived correlation functions.

Some example results of f- and g-type correlations using various estimators are given in figures 8 and 9 respectively.

4 Further derivations

4.1 Length scales and dissipation rate

The obtained correlation functions and the turbulence spectra can be used to derive several time and length scales and also the dissipation rate. This requires spatial correlations and the corresponding wave number spectra, which can be obtained directly using multi-point measurements. Temporal correlation functions and power spectra from single-point measurements first have to be transformed to spatial functions using the Taylor hypothesis

$$\kappa = \frac{\omega}{\bar{u}} \tag{20}$$

$$r = \bar{u}t \tag{21}$$

with the wave number $\kappa = \frac{2\pi}{\lambda}$, the circular frequency $\omega = 2\pi f$, the spatial distance r, the time t and the mean velocity $\bar{u}$, leading to the expressions

$$E(\kappa) = E\left(\frac{2\pi f}{\bar{u}}\right) = \frac{\bar{u}}{2\pi}G(f) \tag{22}$$

$$R_r(r) = R_t\left(\frac{r}{\bar{u}}\right) \tag{23}$$

with the wave number spectrum $E(\kappa)$, the power spectrum $G(f)$, the spatial and the temporal correlation functions $R_r(r)$ and $R_t(\tau)$ with

$$E(\kappa) = \frac{1}{\pi}\int_{-\infty}^{\infty} R_r(x)\cos(\kappa x)\,\mathrm{d}x \tag{24}$$

$$G(f) = 2\int_{-\infty}^{\infty} R_t(\tau)\cos(2\pi f\tau)\,\mathrm{d}\tau \tag{25}$$

$$R_r(x) = \langle u(r)u(r+x)\rangle \tag{26}$$

$$R_t(\tau) = \langle u(t)u(t+\tau)\rangle \tag{27}$$

and the expectation $\langle\rangle$.

For isotropic turbulence and streamwise laser Doppler mesurements, the fit

$$E(\kappa) = 0.49\epsilon^{2/3}\kappa^{-5/3} \tag{28}$$

to the inertial subrange of the wave number spectrum can be used to estimate the dissipation rate of turbulent kinetic energy per unit mass, ϵ.

From a parabolic fit to the spatial correlation function at $x = 0$ the Taylor length scale λ_f (f-type for streamwise measurements) can be computed using

$$\lambda_f^2 = \frac{2\langle u'^2\rangle}{\left\langle \left(\frac{\partial u'}{\partial x}\right)^2 \right\rangle} = -2\frac{R_r(0)}{R_r''(0)} \tag{29}$$

Then the dissipation rate can be estimated using

$$\epsilon = 30\nu\frac{\langle u'^2\rangle}{\lambda_f^2} \tag{30}$$

with the kinematic viscosity ν.

Finally, the dissipation rate can be estimated from the integral length scale

$$L = \frac{1}{\langle u'^2\rangle}\int_0^\infty R_r(x)\,\mathrm{d}x \tag{31}$$

using

$$\epsilon = \frac{k^{3/2}}{2L} \tag{32}$$

and with the turbulent kinetic energy

$$k = \frac{3}{2}\langle u'^2\rangle \tag{33}$$

Note that all these expressions are valid only for isotropic turbulence, small turbulence levels and measurements of the streamwise velocity component.

4.2 Spectral Limits

The discussion in section 3 indicates that the choice of spectral estimator greatly influences the maximum frequency to which the PSD can be reliably estimated. Whereas equally spaced samples yield estimates only up to the Nyquist frequency, i. e. half of the sample rate, the situation with irregularly sampled data is quite variant. A simple sample-and hold reconstruction with re-sampling allows estimates up to $\dot{n}/2\pi$. The more advanced estimators can extend this to several times $\dot{n}$. However $\dot{n}$, the mean data rate, can be increased by either increasing the tracer particle density or by enlarging the measurement detection volume of the system. In both cases, the probability of obtaining two particles simultaneously in the detection volume must be kept low.

Given that this probability is to remain less than 0.5 % and assuming a Poisson distribution, the Poisson parameter $\bar{N}$, expressing the mean number of particles simultaneously in the volume, i. e.

$$P(N,\bar{N}) = \frac{\bar{N}^N}{N!}\mathrm{e}^{-\bar{N}} \tag{34}$$

must satisfy $\bar{N} < 0.1$. If V_0 is the measurement volume, then the allowable concentration c_s (particles/m^3) becomes

$$c_s \le \frac{0.1}{V_0} \tag{35}$$

On the other hand, c_s must be chosen large enough to yield the required mean data rate to estimate the spectrum at the desired maximum frequency $f_{\max}$. Assuming $f_{\max} \le \dot{n}$ (conservative) and using Eq. (2)

$$c_s = \frac{\dot{n}}{A_\perp \bar{u}} \ge \frac{f_{\max}}{A_\perp \bar{u}} \tag{36}$$

Since the right-hand side of Eq. (36) must always be less than that of Eq. (35)

$$f_{\max} \le 0.1\frac{\bar{u}A_\perp}{V_0} \approx \frac{0.3\bar{u}}{r_\mathrm{d}} \tag{37}$$

for an elliptical volume where r_d is the radius of the ellipsoidal detection volume and a one-dimensional flow is assumed. This indicates that the spectral limit in frequency is determined by the dimensions of the measurement volume and the mean velocity and that a corresponding particle density must be chosen to attain this limit.

5 Conclusion

The procedures for estimating power spectral density, autocorrelation function and various quantities derived from these functions from laser Doppler data has been reviewed. Two spectral estimators for single-component, single-point systems have been reviewed. Some remarks about how these estimators can be extended to multi-component or multi-point measurements have been made. Finally, the consequences of using these improved estimation procedures on the layout of the optical system have been briefly discussed.

References

[1] R J Adrian and C S Yao. Power spectra of fluid velocities measured by laser Doppler velocimetry. *Exp. in Fluids*, 5:17–28, 1987.

[2] D O Barnet and H T Bentley. Statistical bias of individual realization laser velocimeters. In *Proc. 2nd Int. Workshop on Laser Velocimetry*, pages 428–444, Purdue University, 1974.

[3] L H Benedict and R D Gould. Understanding biases in the near-field region of LDA two-point correlation measurements. In *Proc. 8th Int. Symp. of Appl. of Laser Techn. to Fluid Mechanics*, Lisbon, Portugal, 1996. paper 36.6.

[4] L H Benedict, H Nobach, and C Tropea. Estimation of turbulent velocity spectra from laser Doppler data. *Meas. Sci. Technol.*, 11(8):1089–1104, 2000.

[5] F Durst and K F Heiber. Signal-Rausch-Verhältnisse von Laser-Doppler-Signalen. *Optica Acta*, 24:43–67, 1977.

[6] R V Edwards and A S Jensen. Particle-sampling statistics in laser anemometers: Sample-and-hold systems and saturable system. *J. Fluid Mech.*, 133:397–411, 1983.

[7] J C Erdmann and C Tropea. Statistical bias of the velocity distribution function in laser anemometry. In *Proc. 1st Int. Symp. on Appl. of Laser Techn. to Fluid Mechanics*, Lisbon, Portugal, 1982. paper 16.2.

[8] W Fuchs, H Nobach, and C Tropea. Laser Doppler anemometry data simulation: Application to investigate the accuracy of statistical estimators. *AIAA Journal*, 32:1883–1889, 1994.

[9] M Gaster and J B Roberts. Spectral analysis of randomly sampled signals. *J. Inst. Maths. Applics.*, 15:195–216, 1975.

[10] M Gaster and J B Roberts. The spectral analysis of randomly sampled records by a direct transform. *Proc. R. Soc. Lond. A.*, 354:27–58, 1977.

[11] W K George and J L Lumley. The laser Doppler velocimeter and its application to the measurement of turbulence. *J. Fluid Mech.*, 60:321–362, 1973.

[12] P Gjelstrup, H Nobach, F Jørgensen, and K E Meyer. Experimental verification of novel spectral analysis algorithms for laser Doppler anemometry data. In *Proc. 10th Int. Symp. on Appl. of Laser Techn. to Fluid Mechanics*, Lisbon, Portugal, 2000. paper 3.2.

[13] W Hösel and W Rodi. New biasing elimination method for laser-Doppler-velocimeter counter processing. *Rev. Sci. Instrum.*, pages 910–919, 1977.

[14] A Høst-Madsen. A new method for estimation of turbulence spectra for laser Doppler anemometry. In *Proc. 7th Int. Symp. on Appl. of Laser Techn. to Fluid Mechanics*, Lisbon, Portugal, 1994. paper 11.1.

[15] W T Mayo Jr, M T Shay, and S Ritter. The development of new digital data processing techniques for turbulence measurements with a laser velocimeter, 1974. AEDC-TR-74-53

[16] H R E van Maanen, H Nobach, and L H Benedict. Improved estimator for the slotted autocorrelation function of randomly sampled LDA data. *Meas. Sci. Technol.*, 10(1):L4–L7, 1999.

[17] H R E van Maanen and A Oldenziel. Estimation of turbulence power spectra from randomly sampled data by curve-fit to the autocorrelation function applied to laser-Doppler anemometry. *Meas. Sci. Technol.*, 9:458–467, 1998.

[18] H R E van Maanen and H J A F Tulleken. Application of kalman reconstruction to laser-Doppler anemometry data for estimation of turbulent velocity fluctuations. In *Proc. 7th Int. Symp. on Appl. of Laser Techn. to Fluid Mechanics*, Lisbon, Portugal, 1994. paper 23.1.

[19] H R E van Maanen and M J Tummers. Estimation of the autocorrelation function of turbulent velocity fluctuations using the slotting technique with local normalization. In *Proc. 8th Int. Symp. on Appl. of Laser Techn. to Fluid Mechanics*, Lisbon, Portugal, 1996. paper 36.4.

[20] D W Marquardt and S K Acuff. *Direct Quadratic Spectrum Estimation with Irregularly Spaced Data*, pages 211–223. Springer Verlag, Berlin, 1983.

[21] D K Mc Laughlin and W G Tiederman. Biasing correction for individual realisation of laser anemometer measurements in turbulent flows. *Phys. of Fluids*, 16(12):2082–2088, 1973.

[22] E Müller, H Nobach, and C Tropea. Model parameter estimation from non-equidistant sampled data sets at low data rates. *Meas. Sci. Technol.*, 9(3):435–441, 1998.

[23] E Müller, H Nobach, and C Tropea. A refined reconstruction-based correlation estimator for two-channel, non-coincident laser Doppler anemometry. *Meas. Sci. and Technology*, 9(3):442–451, 1998.

[24] H Nobach. Processing of stochastic sampled data in laser Doppler anemometry. In *Proc. 3rd International Workshop on Sampling Theory and Applications*, pages 149–154, 1999.

[25] H Nobach, E Müller, and C Tropea. Refined reconstruction techniques for LDA data analysis. In *Proc. 8th Int. Symp. on Appl. of Laser Techn. to Fluid Mechanics*, Lisbon, Portugal, 1996. paper 36.2.

[26] H Nobach, E Müller, and C Tropea. Correlation estimator for two-channel, non-coincidence laser-Doppler-anemometer. In *Proc. 9th Int. Symp. on Appl. of Laser Techn. to Fluid Mechanics*, Lisbon, Portugal, 1998. paper 32.1.

[27] A K P Rajpal. Power spectrum estimates of LDA measurements using scargle periodogram analysis. In *Proc. ASME/JSME Fluids Eng. and Laser Anemometry Conf.*, pages

411–415, Hilton Head Island, South Carolina, USA, 1995. FED-Vol. 229.

[28] J B Roberts, J Downie, and M Gaster. Spectral analysis of signals from a laser Doppler anemometer operating in the burst mode. *J. Phys. E: Sci. Instrum.*, 13:977–981, 1980.

[29] P Saarenrinne, S Soini, H Ihalainen, and O Kaleva. Turbulence spectral power density estimation for laser Doppler anemometer measurements in a mixing tank flowfield. In *Proc. 7th Int. Conf. on Laser Anemometry*, pages 335–342, Karlsruhe, 1997.

[30] J D Scargle. Studies in astronomical time series analysis. ii. statistical aspects of spectral analysis of unevenly spaced data. *The Astrophysical Journal*, 263:835–853, 1982.

[31] M J Tummers and D M Passchier. Spectral estimation using a variable window and the slotting technique with local normalization. *Meas. Sci. Technol.*, 7:1541–1546, 1996.